GLRT-BASED ADAPTIVE DOPPLER PROCESSING FOR HF RADAR SYSTEMS

Giuseppe A. Fabrizio

Signal Processing and Propagation Group,
ISR Division, DSTO Australia.

Alfonso Farina

SELEX Sistemi Integrati (SELEX-SI),
Via Tiburtina, km 12.4, 00131, Rome, Italy.

ABSTRACT

High frequency skywave and surface-wave over-the-horizon (OTH) radars are required to detect targets in the presence of powerful clutter and interference from man-made and natural sources. However, the received disturbances may be highly structured in the time domain (i.e. pulse-to-pulse) within the coherent processing interval (CPI). This provides scope for adaptive Doppler processing to enhance detection performance with respect to conventional FFT-based methods. This paper proposes a Generalized Likelihood Ratio Test (GLRT) based detector that not only possesses the valuable Constant False Alarm Rate (CFAR) property invariant to disturbance scale-change, but also exhibits distinct advantages over the adaptive coherence estimator (ACE) and adaptive subspace detector (ASD) when unwanted signals are present. Here, we present the first experimental results for this detector in a HF surface wave radar Doppler processing application.

Index Terms— Adaptive Signal Detection, HF Radar

1. INTRODUCTION

A significant signal processing challenge for modern HF radar systems is the simultaneous detection and tracking of ships and aircraft on different carrier frequencies. Ship detection may require very long coherent processing intervals (CPIs) to resolve targets against clutter using conventional FFT-based Doppler processing (e.g. 30-60 seconds). Such long CPI's heavily consume radar resources and prevent the radar from performing other functions, such as revisiting aircraft targets sufficiently often to allow tracking. For this reason, there is currently great interest in performing ship detection with much shorter CPIs (e.g. 10-20 seconds). We note that apart from the limited Doppler resolution, conventional processing is also sub-optimal for temporally correlated interference.

As the received clutter and interference may be highly structured in the time domain (pulse-to-pulse) within the CPI, adaptive Doppler processing can potentially enhance target detection relative to data-independent processing. The goal of many adaptive processors is to improve the probability of detection while maintaining a constant false alarm rate, this is especially desirable in heterogenous environments where the disturbance is not identically distributed across all of the resolution cells in the radar coverage.

Unlike the adaptive matched filter (AMF) [1] and Kelly's GLRT [2], that are CFAR strictly for an identically Gaussian distributed disturbance in the primary and secondary data, the ACE detector [3] maintains the CFAR property providing the disturbance in the test cell and training data have the same covariance structure, but possibly with different level or scale. This additional invariance is attractive as it provides a further degree of protection in practical situations of interest when the CFAR output can be lost due to this phenomenon [4].

However, ACE is known to discriminate strongly against mismatched signals, and this is a problem for useful signals not exactly described by the assumed target model; either due to environmental factors (e.g multipath) and/or instrumental imperfections (e.g. array calibration errors). An extension of ACE assumes a multi-rank or subspace signal representation that is more robust to a partially unknown target response. These adaptive subspace detectors (ASDs) were derived in [5]. Despite their appeal, a significant shortcoming of the ACE and ASD tests is that they are susceptible to unwanted signals present in the primary data but not in the secondary data. Such signals can cause masking of desired signals and preclude their detection [4].

The paper exposes this latent susceptibility in practice and proposes a GLRT-based detection scheme to prevent useful signal masking when unwanted signals are present. Section 2 formulates the detection problem, while section 3 describes the adaptive detection method. Experimental results follow in section 4, and conclusions are given in section 5.

2. PROBLEM FORMULATION

The *primary* inputs to the Doppler processor consist of P complex samples $x(t)$ for $t = 1, 2, \ldots, P$ received over P pulses in the range-azimuth cell under test (CUT). In our case, the generalized problem includes unwanted signals such that the data vector $\mathbf{x} = [x(1), \ldots, x(P)]^T$ is modeled as,

$$\begin{cases} H_0: & \mathbf{x} = \mathbf{s}_u + \mathbf{d}, \\ H_1: & \mathbf{x} = \mathbf{s}_d + \mathbf{s}_u + \mathbf{d}. \end{cases} \tag{1}$$

Under the null hypothesis H_0, $\mathbf{x}$ is the superposition of a Gaussian disturbance $\mathbf{d}$ and a deterministic unwanted signal $\mathbf{s}_u$ confined to the CUT (e.g. a coherent echo with Doppler components significantly different to the target). Under the alternative hypothesis H_1, the useful signal $\mathbf{s}_d$ is also present. Ideally, $\mathbf{s}_d = \mu e^{j\theta}\mathbf{v}(f_d) = \mu e^{j\theta}[1, e^{j2\pi f_d}, \ldots, e^{j2\pi(P-1)f_d}]^T$, where $\mu e^{j\theta}$ is the unknown complex amplitude of the target and f_d is the Doppler frequency shift normalized by the pulse repetition frequency (PRF). In practice, targets may exhibit some degree of Doppler spread or mismatch, and a subspace model may be more appropriate. Targets may be represented by a linear combination of Q complex phasors closely spaced in Doppler frequency. By defining a low-rank subspace model $\mathbf{H} = [\mathbf{v}(f_d), \mathbf{v}(f_d + \delta_2), \ldots, \mathbf{v}(f_d + \delta_Q)]$, with $Q \ll P$, and letting $\underline{\theta}$ be the unknown parameter vector, we can express $\mathbf{s}_d$ in the following general form.

$$\mathbf{s}_d = \mathbf{H}\underline{\theta} \tag{2}$$

The unwanted signal may arise from a clutter discrete or other target with a Doppler shift different to the one being tested by the detector. A low-rank subspace model can also be adopted for $\mathbf{s}_u$, as in [6], with $\mathbf{S} = [\mathbf{v}(f_u), \mathbf{v}(f_u+\delta_2), \ldots, \mathbf{v}(f_u+\delta_Q)]$ centered on the unwanted signal Doppler shift f_u, and $\underline{\phi}$ as the unknown parameter vector.

$$\mathbf{s}_u = \mathbf{S}\underline{\phi} \tag{3}$$

The disturbance $\mathbf{d}$ may consist of clutter and/or interference. Sea clutter is dominated by first-order scatter from ocean wave components called Bragg waves. In essence, the advance and recede Bragg waves produce discrete Doppler components known as Bragg lines [7]. HF interference may originate from natural sources, such as lightning, or man-made sources such as radio broadcasts. Lightning discharges are impulsive and contaminate all range cells in a number of radar pulses within the CPI. Similarly, the instantaneous bandwidth of man-made sources can change rapidly and overlap the radar bandwidth only at certain times, contaminating all range cells but only in a subset of the P pulses. Both types of disturbance have temporal structure that can be "learned" from secondary data vectors $\mathbf{d}_k$ for $k = 1, \ldots, K$ taken from resolution cells close to the CUT. These vectors are assumed mutually independent with the same covariance structure as the disturbance in the primary data. The unknown relative disturbance level being assigned a value σ^2. Such a description (4) is known to be especially applicable when clutter or interference dominates [4].

$$\mathbf{E}\{\mathbf{d}\mathbf{d}^\dagger\} = \sigma^2\mathbf{E}\{\mathbf{d}_k\mathbf{d}_k^\dagger\} = \sigma^2\mathbf{R} \tag{4}$$

3. ADAPTIVE DETECTION METHOD

Under these assumptions, $\mathbf{x}$ has a density function $f_{\mathbf{x}|H_\gamma}(\mathbf{x})$ conditioned on σ^2 for the hypothesis in force ($H_\gamma : \gamma = 0, 1$).

$$f_{\mathbf{x}|H_\gamma}(\mathbf{x}) = \frac{1}{(\pi\sigma^2)^P\|\mathbf{R}\|}e^{\{-\frac{1}{\sigma^2}(\mathbf{x}-\mathbf{m}_\gamma)^\dagger\mathbf{R}^{-1}(\mathbf{x}-\mathbf{m}_\gamma)\}} \tag{5}$$

Here, $\mathbf{m}_\gamma = \gamma\mathbf{H}\underline{\theta} + \mathbf{S}\underline{\phi}$, and $\|\cdot\|$ denotes determinant. Since the likelihood ratio test cannot be implemented due to the unknown distributional parameters $(\sigma^2, \mathbf{R}, \underline{\theta}, \underline{\phi})$, we resort to the GLRT method to derive a detector based on maximizing the joint density function of the primary and secondary data $f_\gamma(\mathbf{x}, \mathbf{d}_1, \ldots, \mathbf{d_k}) = f_{\mathbf{x}|H_\gamma}(\mathbf{x})\prod_{k=1}^{K}\frac{1}{\pi^P\|\mathbf{R}\|}\ e^{\{-\mathbf{d}_k^\dagger\mathbf{R}^{-1}\mathbf{d}_k\}}$ with respect to these parameters under each hypothesis.

$$\frac{\max_{\sigma^2,\mathbf{R},\underline{\theta},\underline{\phi}}\ f_1(\mathbf{x}, \mathbf{d}_1, \ldots, \mathbf{d}_K)}{\max_{\sigma^2,\mathbf{R},\underline{\phi}}\ \ f_0(\mathbf{x}, \mathbf{d}_1, \ldots, \mathbf{d}_K)} \underset{H_0}{\overset{H_1}{\gtrless}} \eta \tag{6}$$

Maximizing $f_1(\mathbf{x}, \mathbf{d}_1, \ldots, \mathbf{d}_K)$ with respect to $\mathbf{R}$ and σ^2 yields the following expression [3],

$$\frac{(K+1)^{(P-1)(K+1)}(K-P+1)^{K-P+1}(KP)^P}{(e\pi K)^{P(K+1)}\|\hat{\mathbf{R}}\|^{K+1}[(\mathbf{x}-\mathbf{m}_1)^\dagger\hat{\mathbf{R}}^{-1}(\mathbf{x}-\mathbf{m}_1)]^P} \tag{7}$$

where $\hat{\mathbf{R}} = \frac{1}{K}\sum_{k=1}^{K}\mathbf{d}_k\mathbf{d}_k^\dagger$ is the full rank ($K > P$) *sample* covariance matrix (SCM). If we maximize $f_0(\mathbf{x}, \mathbf{d}_1, \ldots, \mathbf{d}_K)$ with respect to the same two parameters, a similar expression results with $\mathbf{m}_1$ replaced by $\mathbf{m}_0 = \mathbf{S}\underline{\phi}$ in (7).

$$\frac{\max_{\sigma^2,\mathbf{R}}\ f_1(\cdot)}{\max_{\sigma^2,\mathbf{R}}\ f_0(\cdot)} = \left\{\frac{(\mathbf{x}-\mathbf{m}_0)^\dagger\hat{\mathbf{R}}^{-1}(\mathbf{x}-\mathbf{m}_0)}{(\mathbf{x}-\mathbf{m}_1)^\dagger\hat{\mathbf{R}}^{-1}(\mathbf{x}-\mathbf{m}_1)}\right\}^P \tag{8}$$

By defining $\mathbf{z} = \hat{\mathbf{R}}^{-1/2}\mathbf{x}$, $\mathbf{\Omega} = \hat{\mathbf{R}}^{-1/2}\mathbf{S}$, $\mathbf{\Psi} = \hat{\mathbf{R}}^{-1/2}[\mathbf{H}, \mathbf{S}]$, and projections $P_{\mathbf{\Psi}} = \mathbf{\Psi}(\mathbf{\Psi}^\dagger\mathbf{\Psi})^{-1}\mathbf{\Psi}^\dagger$, $P_{\mathbf{\Omega}} = \mathbf{\Omega}(\mathbf{\Omega}^\dagger\mathbf{\Omega})^{-1}\mathbf{\Omega}^\dagger$, the P^{th} root of the GLRT takes the following form [8]:

$$\frac{\mathbf{z}^\dagger(\mathbf{I}-\mathbf{P_\Omega})\mathbf{z}}{\mathbf{z}^\dagger(\mathbf{I}-\mathbf{P_\Psi})\mathbf{z}} \underset{H_0}{\overset{H_1}{\gtrless}} \gamma \tag{9}$$

This detector represents a generalization of the results in [3] for overall disturbances modeled by a deterministic low-rank subspace component $\mathbf{s}_u = \mathbf{S}\underline{\phi}$ and a statistical "colored" component $\mathbf{d}$. This GLRT assumes the subspace $\mathbf{S}$ is known, but in practice, it must be estimated. We propose to make a first pass assuming $\mathbf{S} = 0$, this detector actually corresponds to a monotone function of the ACE ($Q = 1$) or ASD ($Q > 1$) tests. Any detections made during the first pass are stored along with their Doppler coordinate f_u. If these detections are at Doppler bins different to the ones interrogated during the second pass (i.e. $f_u \neq f_d$), the detector in (9) is used to process such cells with an appropriate unwanted signal model (3). The aim of the second pass is to uncover any new targets that may have been masked by unwanted signals during the first pass.

4. EXPERIMENTAL RESULTS

Data Collection: Experimental data were collected by a 16 channel uniform linear array of monopole receiving elements in the Iluka HFSW radar, located near Darwin in far north Australia [4]. Each CPI is approximately 16 seconds long and consists of $P = 32$ sweeps (pulses) of a linear frequency modulated continuous waveform with a center frequency $f_c =$

7.719 MHz, bandwidth $B = 50$ kHz and a pulse repetition frequency (PRF) $f_p = 2$ Hz. A total of $L = 40$ range cells were processed in 16 conventional beams. Some high Doppler resolution CPI with $P = 128$ sweeps (64 s long) were recorded for identifying targets of opportunity.

High Resolution Spectra: Fig. 1(a) shows an intensity modulated range-Doppler display for a beam containing three targets of opportunity. Doppler bins are arranged horizontally and range cells vertically. Red indicates high power and blue indicates low power. Conventional Doppler processing was applied to a 64 second CPI using a Blackman-Harris window. A number of features are indicated in the display, in particular the existence of three targets (labelled T1,T2 and T3). Note that T2 and T3 are in the *same* range-azimuth cell but have quite different Doppler shifts. A cell-averaging constant false alarm rate (CFAR) technique is then applied to normalize the clutter prior to threshold detection. This is shown in Fig. 1(b) where all three targets can be detected using the long CPI (with some false alarms due to clutter near the direct wave).

Impact of Short CPI and Interference: Fig. 2, in the same format as Fig. 1, shows the conventional processing output for a short CPI (16 seconds) when interference is present. In this case, FFT-based processing is not able to detect any targets, as only the direct wave return is visible after CFAR processing. Using the same data, Fig. 3 shows the output of the ACE and ASD tests using $Q = 3$ for the latter with half Doppler frequency bin displacements $\delta_2 = \pi/P$ and $\delta_3 = -\pi/P$. The disturbance sample covariance matrix $\hat{\mathbf{R}}$ is formed using $K = 4P = 128$ snapshots neighboring the CUT in range and beam (with one guard cell in each dimension). The ACE test detects T1 and T2, but misses T3 in Fig 3(a) with a detection threshold of 5 dB. The ASD output in Fig. 3(b) also misses T3, but performs better on T1 with slightly inferior clutter suppression near the direct wave. These displays represent the first pass for the generalized adaptive detection schemes.

Generalized Detectors: The generalized adaptive detector (9) was applied using Q=1 (G-ACE), and $Q = 3$ (G-ASD). The detections made during the first pass, in Figs.3(a) and (b) respectively, were used to form the unwanted signal model (3) for the generalized tests in an attempt to uncover other signals possibly masked by the detected targets T1 and T2. Fig. 4(a) shows that G-ACE was unsuccessful in uncovering T3, possibly due to this target (and T2) not being sufficiently well modeled by a single complex phasor. On the other hand, it is evident from Fig. 4(b), that the G-ASD detector detects all the targets with a short CPI in the presence of interference. Its ability to outperform G-ACE may be due to the robust model for the undesired and desired signals in the CUT. The Doppler profiles in Fig. 5 clearly show the advantage of G-ASD over the ASD in the two range cells containing the targets. While the ASD performs very well when the CUT contains a single target (range 18), it fails to detect both targets in range 15. The G-ASD explicitly takes unwanted signals into account and is able to detect all targets T1, T2 and T3.

5. CONCLUSIONS

This paper has presented and experimentally tested a robust adaptive Doppler processing method for ship detection with short CPI in HFSW radar. The GLRT-based detection method generalizes ACE and ASD by including subspace unwanted signals to the overall disturbance. When unaccounted for, such signals that have the potential to mask targets in the CUT when ACE or ASD tests are applied. The generalized ASD (G-ASD) detector was found to be most effective, and unlike the standard ACE or ASD tests, clearly showed its ability to detect two targets in the same CUT. The G-ACE version was not as robust as G-ASD, perhaps due to its inability to model the unwanted and desired signals well enough, combined with the highly selective nature of the test. The practical benefits of the G-ASD are not limited to HFSW radar (or Doppler processing). It is envisaged that this technique can be applied to sky-wave OTH radar, and possibly other radar systems, also in the areas of spatial processing and space-time adaptive processing (STAP) [9].

6. REFERENCES

[1] F. C. Robey, D. R. Fuhrmann, E. J. Kelly, R. Nitzberg; "A CFAR adaptive matched filter detector," *IEEE Transactions on Aerospace and Electronic Systems*, Vol.28, No.1, January 1992, pp. 208-216.

[2] E. J. Kelly; "An adaptive detection algorithm," *IEEE Transactions on Aerospace and Electronic Systems*, Vol.22, No.1, March 1986, pp. 115-127.

[3] S. Kraut, L. L. Scharf; "The CFAR adaptive subspace detector is a scale-invariant GLRT," *IEEE Transactions on Signal Processing*, Vol.47(8), 1999, pp. 2538-2541.

[4] G. A. Fabrizio, A. Farina, M. Turley; "Spatial Adaptive Subspace Detection in OTH Radar," *IEEE Transactions on Aerospace and Electronic Systems*, Vol.39, No.4, 2003, pp. 1407-1427.

[5] S. Kraut, L. L. Scharf, T. McWhorter; "Adaptive subspace detectors," *IEEE Trans. on Signal Processing*, Vol.49, No.1, January 2001, pp. 1-16.

[6] L. L. Scharf, M. L. McCloud; "Blind adaptation of zero forcing projections and oblique pseudo-inverses for subspace detection and estimation when interference dominates noise," *IEEE Trans. on Signal Processing*, Vol.50, No.12, December 2002, pp. 2938-2946.

[7] B. J. Lipa, D. E. Barrick; "Extraction of sea-state from HF radar sea echo: mathematical theory and modeling", *Radio Science*, Vol. 21, No. 1, 1986, pp 81-100.

[8] G. A. Fabrizio, L. L. Scharf, A. Farina, M. D. Turley; "Ship detection with HF surface wave radar using short integration times," *International Radar Conference*, IEEE, Toulouse, France, October 2004.

[9] G. A. Fabrizio, G. J. Frazer, M. D. Turley; "STAP for clutter and interference cancellation in a HF radar system," *ICASSP-06*, Toulouse, France, May 2006.

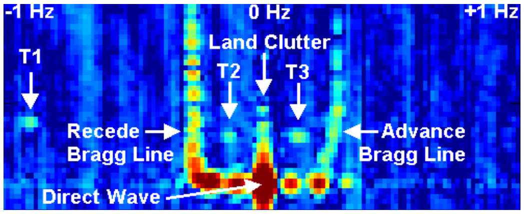

(a) Range-Doppler map for beam with targets of opportunity.

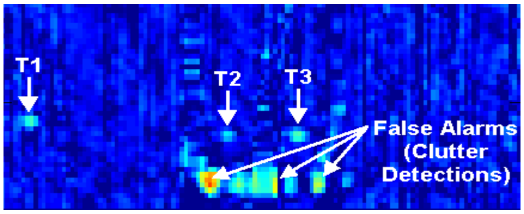

(b) Range-Doppler map after cell-averaging CFAR processing.

Fig. 1. Conventional output with high Doppler resolution.

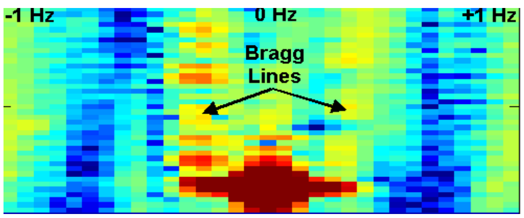

(a) Range-Doppler map for beam with targets of opportunity.

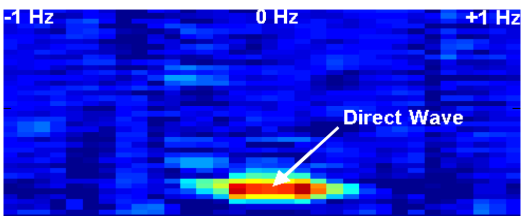

(b) Range-Doppler map after cell averaging CFAR processing.

Fig. 2. Conventional output with short CPI and interference.

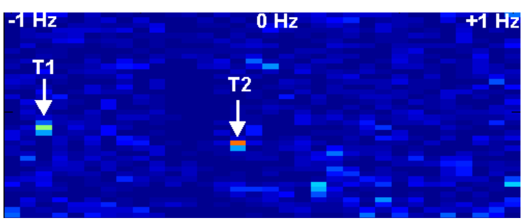

(a) Adaptive Coherence Estimator (ACE)

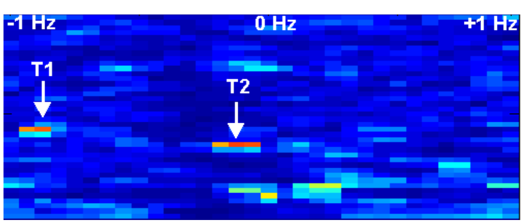

(b) Adaptive Subspace Detector (ASD)

Fig. 3. Adaptive outputs for short CPI with interference.

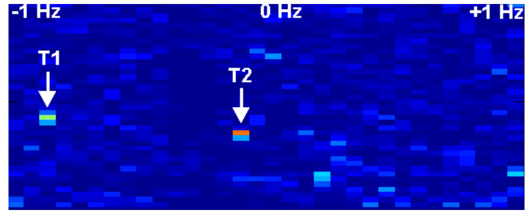

(a) Generalized Adaptive Coherence Estimator (G-ACE).

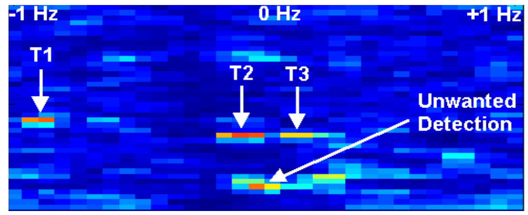

(b) Generalized Adaptive Subspace Detector (G-ASD).

Fig. 4. Output of proposed generalized detection methods.

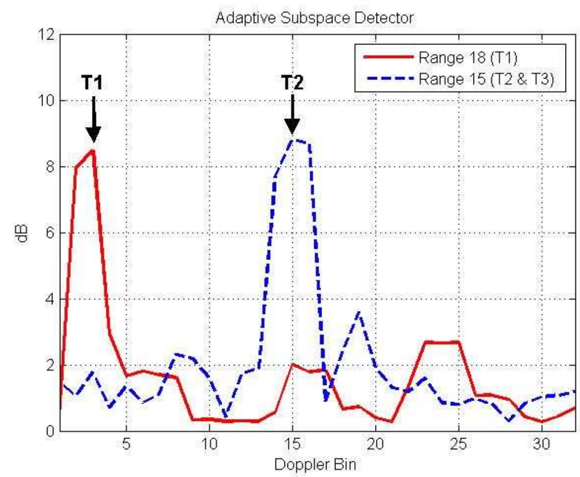

(a) Adaptive Subspace Detector

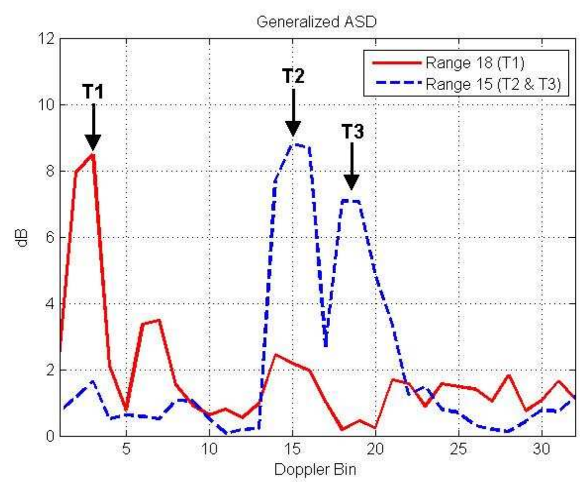

(b) Generalized Adaptive Subspace Detector

Fig. 5. Doppler profiles for range cells containing targets.